Design and Numerical Analysis of a Twin-Rotor Axial-Inflow Air Turbine with Self-Rectifying Valves for Wave Energy Converters

Ana Catarina Louro Paralta
catarinaparalta@tecnico.ulisboa.pt

Instituto Superior Técnico, Universidade de Lisboa, Portugal

July 2017

Abstract

The research and development of wave energy converters is encouraged by the current energy market tend to increase renewable energy sources quota due to the environmental impact of fossil energy sources. Although the concept of oscillating water column is well established as the most common method for wave energy conversion, the choice of turbine to be used on this device is still a relevant investigation topic. High efficiencies and wide operating ranges make unidirectional turbines worth noticing. This thesis consists in the design and numerical analysis of a reaction turbine stage. From an initial one-dimensional analysis, it is possible to obtain the flow velocity triangles. Through an inverse design method on the assumption of potential flow, the two-dimensional blade mean line is iterated until the required flow characteristics are verified. The flow upstream the stator is assumed to be axial and uniform, consequently, a known thickness distribution is applied to this component. Since a wave energy device requires a wide range of operating conditions, the rotor thickness distribution is optimized for a certain pressure coefficient distribution which allows the deviation of the inlet flow angle without a significant impact on efficiency. A numerical analysis of the two-dimensional and three-dimensional viscous flow is, then, required to verify the previous design process. ANSYS Fluent and ANSYS CFX are used. The performance map for the designed turbine successfully exhibited a high peak efficiency as predicted and, additionally, a wide flat operating range appropriate for a wave energy converter.
Keywords: Wave Energy, Oscillating Water Column, Twin-Rotor Axial-Inflow Turbine, Reaction Turbine, Computational Fluid Dynamics

1. Introduction

Wave energy conversion presence in the renewable energy global usage panorama is still very residual. Although the exploitable potential of wave energy is around $10 - 25\%$ of the world electricity consumption [1], wave energy converters are not yet an economically viable energy source.

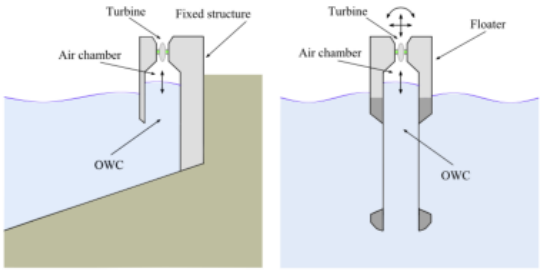

Figure 1: OWC configuration. Retrieved from [3].

Simplicity allied with high efficiencies make oscillating water column (OWC) devices one of the most extensively studied and tested wave energy converters, [2]. Based on a pneumatic system with air in an open-circuit or closed-circuit, the OWC has an internal air chamber limited by a air turbine above sea level and by a water-air interface below. Since the device is open below sea level, wave action will cause the movement of the interface and, consequently, the pressure on the chamber will vary. Alternate compression and decompression will force the air through the turbine which is coupled to a generator. OWC installation may be on a fixed or floating structure, Figure 1.

Since the OWC and the generator already guarantee a high efficiency performance, to increase the efficiency of the turbine is of major importance. Several unidirectional and bidirectional axial-flow turbines have been developed and tested. The absence of a rectifying valve system makes bidirectional turbines, thus self-rectifying, more attractive both economically and practically since large devices require small response times. Regarding self-rectifying air turbines, the Wells turbine and the impulse turbine have high relevance in OWC appli-

cations. Characterized by a narrow operating range and high aerodynamic losses on the second row of guide vanes, respectively, these turbine types also feature low values of peak efficiency.

A twin-rotor axial-inflow air turbine represents an alternative to the previous mentioned turbines. Eliminating low efficiency limitations and narrow operating ranges, [4], this configuration consists in two turbines in parallel coupled a common generator or not. Both turbines are unidirectional since the intake air flow goes through one turbine while the exhaust air flow goes through the other. However, the duplication of the turbine and channels system implies a significant economical drawback.

The main objective of this work is to design and perform a numerical analysis of a stator and rotor axial assembly to be applied on a twin-rotor axial-inflow air turbine configuration. The final efficiency curve assessment will be determinant to conclude if the performance of the obtained design is satisfactory enough to overcome economical impact of this solution.

2. Methodology

The design process for axial turbines as been intensively studied in the past motivated mostly by the aeronautical and power generation industries. A wide variety of methods is, consequently, available and the method choice depends not only on the precision required but also on the computational capability available.

Geometry constraints for the current project imply a high hub radius to tip radius ratio, therefore, the assumption of bidimensional flow is acceptable, [5]. Three blade profiles will, then, be designed each one located at a specific spanwise location: 10% span, mean radius which corresponds to approximately 54.7% span and 90% span. The extreme locations were chosen to minimise the influence of the turbine casing walls on the design.

2.1. Preliminary Design

From the spanwise locations chosen, the mean radius is the least affected by the wall casing effects which implies that the efficiency of the energy transfer between the rotor blade and the flow is maximum. Therefore, the flow characteristics imposed during design phase at the mean radius will limit the global turbine efficiency.

A 50% reaction is demanded at the mean radius given the advantage of having symmetrical velocity triangles at the stator outlet and at the rotor outlet, Figure 2. Performance charts obtained through loss estimation correlations for 50% reaction axial stage turbines from [6] are used to select the flow coefficient. Assuming an axial inlet flow and opting for the highest flow coefficient value, in order to obtain a compact geometry, the flow angles required across the stage are set for the mean radius location. The pitch to chord ratio between two consecutive profile blades has a significant impact on the losses accounted across the passage, consequently, the Zweifel criterion is adopted as an initial design condition.

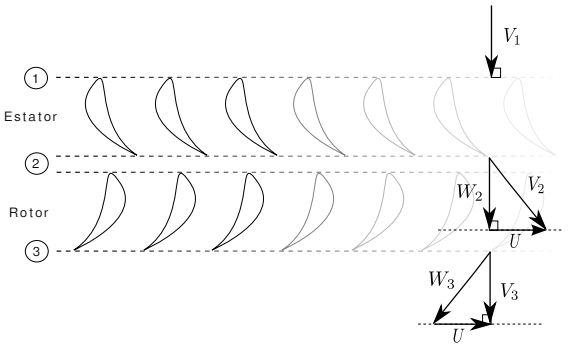

Figure 2: Typical configuration of a midspan section of a 50% reaction turbine.

With the flow conditions defined for the mean radius, a method is required to predict the flow variation along the spanwise direction. The Radial Equilibrium Theory allows a prediction of the impact of the radial velocity, not assumed previously, on the tangential and axial velocity variation. The flow is assumed to be in radial equilibrium along the streamwise direction except within the blade row, which is not true in real flow since the radial equilibrium is only ideally verified at an infinite distance from the blade row position. Consequently, the Radial Equilibrium Theory results require a correction to allow a continuous variation of the radial and axial velocities across the blade row as well as to capture the interaction effects between the stator and rotor blade rows. This method is termed Actuator Disc Approach. Finally, the flow angle variation needed to perform the two-dimensional blade profile design may be obtained, Figure 3.

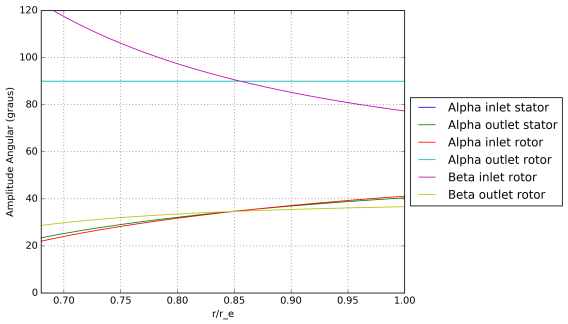

Figure 3: Velocity angle spanwise distribution for relevant design streamwise locations.

2.2. Camber line design method

Based on [7], an inverse method is used to design the profile geometry. Although this type of methods require the flow characteristics to be known a-priori, they are notably robust and fast to achieve convergence from an initial geometry guess.

The process of camber line curvature design consists in a method of potential flow calculation across a blade cascade integrated within a camber line calculation algorithm which updates the geometry in each iteration according to the deviation between the actual flow and the required flow.

For a given thickness distribution, the algorithm illustrated on Figure 4 starts with a guess of the mean flow angle, the camber line curvature and the mass averaged tangential velocity at the outlet. The potential flow calculation step outputs the surface tangential velocity distribution along the chord and the flow angles, essential to iterate each of the mentioned parameters.

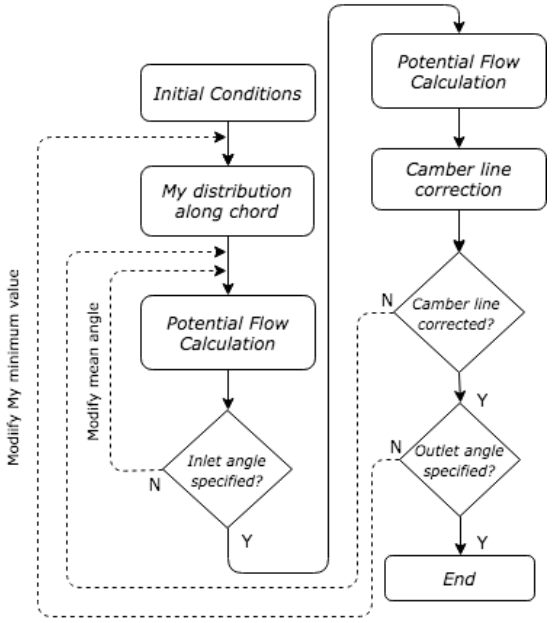

Figure 4: Camber line design algorithm.

From the momentum balance across the tangential direction in steady state, the mass averaged tangential velocity, $\bar{M}_y$, variation across the blade passage is related to the pressure difference between the suction and pressure surface, Δp, through Equation 1 where $\dot{m}$ corresponds to the mass flow. Hence, the distribution of this variable will have a significant impact on the two-dimensional losses which are highly dependent on the surface pressure distribution, namely friction and separation losses. Since the limit values of this function are defined by the inlet and outlet flow angles, the shape of the curve between those must be specified as a criterion. A constant distribution was adopted for the pressure loading, therefore, the $\bar{M}_y$ distribution is linear except near the leading and trailing edges where the curve derivatives must be zero and a cubic polynomial function was used.

$$-\frac{\Delta p}{\dot{m}} = \frac{\mathrm{d}\bar{M}_y}{\mathrm{d}x} \tag{1}$$

The correction of the camber line tangent at a certain position, $\tan\theta$, can be related with the deviation between the specified $\bar{M_y}^{sp}$ and the actual iteration $\bar{M_y}^{n}$, Equation 2 where n stands for the iteration number and ω is a relaxation number. Given the tangent correction, the camber line can now be modified.

$$\tan\theta^{n+1} = \tan\theta^{n} + \omega\left[\bar{M_y}^{sp} - \bar{M_y}^{n}\right] \tag{2}$$

2.3. Blade thickness distribution optimization method

Although the pressure loading distribution is already defined, the surface pressure distribution is still dependent on the thickness distribution applied. An ideal pressure coefficient distribution does not exist, therefore, a criterion for this parameter must be selected taking into account the loss minimisation target. Some common distributions may be found in [8]. Given the requirements for a OWC turbine, a zero pressure gradient distribution was initially studied, followed by a favourable pressure gradient distribution.

The thickness optimization method adopted here was retrieved from [3]. It consist in a differential evolution algorithm where a significant sample of vectors, in which each component corresponds to a normal thickness value, is analysed through a objective function chosen. Vectors with favourable values for the objective function are passed to the next generation, while the rest is rejected. The next generation will be composed of mutations, crossovers and selection between these vectors. The process is repeated until the vector which reveals the minimum value for the objective function is found.

For the constant pressure coefficient distribution, the objective function quantifies the deviation of the tangential velocity in each point when compared to the mean value and to the maximum value. Posteriorly, for the favourable pressure gradient distribution the objective function quantifies the deviation of the tangential velocity in each suction surface point when compared to a line traced between a pressure coefficient point near the leading edge and a point near the trailing edge.

2.4. Computational Fluid Dynamic Method

To access the flow losses associated with each geometry during the design phase, the simulation of the two-dimensional steady-state flow across the

blade passage is required. The comparison of performance results, namely the drag coefficient result, between the different geometries will allow the selection of the geometry that better fits the turbine requirements. The drag coefficient for a blade cascade in incompressible flow is defined by Equation 3 where D is the drag force, ρ is the fluid density, V_m is the mean velocity and c is the blade chord.

$$C_d = \frac{D}{\frac{1}{2}\rho V_m^2 c} \tag{3}$$

Posteriorly, the simulation of the three-dimensional flow across the turbine passage is done in order to verify the agreement of the design procedure assumptions with three-dimensional flow effects. The commercial software ANSYS Fluent 6.3 and ANSYS CFX 18.0 will be used to execute the two-dimensional and three-dimensional analysis, respectively.

Although a computational fluid dynamic simulation solution will inevitably have a deviation when compared to the real flow situation, the modelling conditions applied must be adequate in order to minimise this deviation. Namely, the domain definition along with the boundary conditions adopted, the mathematical model used to solve the flow and the grid configuration applied over the domain will have a significant impact on the final solution.

According to the known flow characteristics across the turbine, the inlet and outlet boundary conditions defined were the magnitude of the inlet velocity axial and the static outlet atmospheric pressure, respectively. Both conditions require a significant distance between the physical boundary and the blade to minimise the influence of blade presence on the flow near these boundaries.

The domain size choice is reflected directly on the computational time required, so, a periodic boundary was used to model the blade cascade. By assuming similar flow characteristics on the two frontiers associated with this boundary type, this condition allows a drastic reduction of the domain size since only one blade passage will be calculated.

Additionally, the three-dimensional calculation requires a condition to model relative movement on the interface between the stator and the rotor. Through circumferentially averaging the flow properties between the steady vane passage and the rotating blade passage, a mixing-plane interface allows a proper modelling and, thus, is applied.

Given the assumption of turbulent flow across the blade passage, the Reynolds-Averaged Navier Stokes equations are used perform the numerical analysis of the flow. By time-averaging the equations of motion for fluid flow, the continuity equation and the momentum equation result in Equation 4 and 5 for steady and incompressible flow, where $\bar{u_i}$ corresponds to the mean velocity, ρ to the fluid density, $\bar{p}$ to the mean pressure and $-\rho\overline{u_i' u_j'}$ to the Reynolds stress tensor.

$$\frac{\partial \bar{u_i}}{\partial x_i} = 0 \tag{4}$$

$$\bar{u_j}\frac{\partial \bar{u_i}}{\partial x_j} = -\frac{1}{\rho}\frac{\partial \bar{p}}{\partial x_i} + \nu\frac{\partial^2 \bar{u_i}}{\partial x_i \partial x_j} + \frac{1}{\rho}\frac{\partial}{\partial x_j}\left(-\rho\overline{u_i' u_j'}\right) \tag{5}$$

The previous equations are not enough to solve the flow and a turbulence model must be adopted to calculate the last term of the momentum equation. The $k-\omega$ SST model is used since its flow behaviour prediction for complex boundary layer flows under adverse pressure gradient and separation is suitable, [9].

The two-dimensional grid is characterised by a C-O topology near the blade wall while the rest of the domain is characterised by a non-structured mesh. However, the three dimensional mesh differs from this configuration once the mesh domain around the C-O topology is structured. Special attention is required regarding the distance of the first node from the wall, the global aspect ratio of the elements and the size ratio between two consecutive elements.

3. Stator Design

The stator geometry must guarantee not only the required flow deflection but also the minimum wake effect downstream possible, since these factors will influence the energy transfer across the rotor directly.

Although the design of the upstream duct the turbine is not covered in the scope of this work, the flow at the inlet of the stator is considered to have exclusively an axial velocity component. Consequently, a typical blade thickness distribution for axial flow turbomachinery applications may be considered. Characterised by small leading edge radius, these distributions are widely used and know to achieve noteworthy performances, [10]. The thickness distributions analysed are presented in Figure 5 where each one exhibits the camber line curvature which allows the flow deflection required in potential flow.

The drag coefficient results for numerical study of the two-dimensional viscous flow across the blade passage with a pitch to axial chord ratio defined by the Zweifel criterion are presented on Table 1.

Table 1: Drag coefficients for each thickness distribution analysed.

	A3K7	B1E1I1	C4	NACA6510	T6
C_d	0.034	0.036	0.032	0.030	0.030

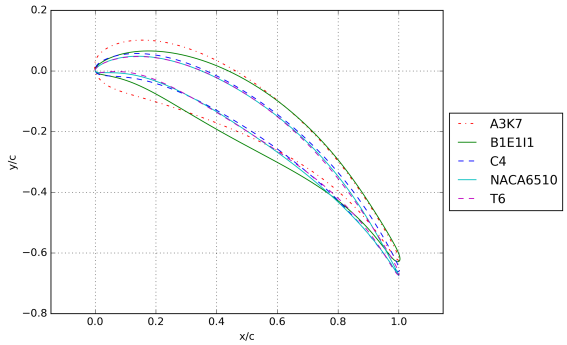

Figure 5: Blade thickness distributions analysed.

The NACA6510 and T6 thickness distributions have the lowest drag coefficient. From a comparison between the pressure distribution for these two geometries, Figure 6, it is possible to conclude that the pressure recovery on the suction near the trailing edge has a higher adverse pressure gradient for the NACA6510 than for the T6 thickness distribution.

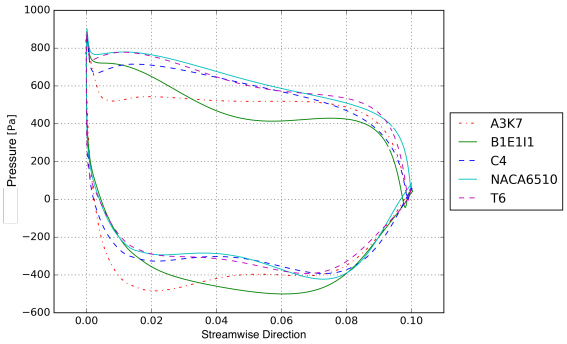

Figure 6: Total pressure distribution for each blade thickness distribution.

Therefore, the thickness distribution T6 is selected for the stator geometry since it represents the geometry with the most adequate performance for the required flow conditions.

The value of the pitch to axial chord ratio, t/b, highly influences the cascade performance. If the ratio value is small, the flow guidance across the blades will be high, but the friction losses will also be high due to the increase in velocity. On the other hand, a large ratio will allow less friction losses, but the flow guidance will be poor and might cause losses due to flow separation. Despite the recommended Zweifel criterion, which states an optimum pitch to axial chord ratio for overall loss minimisation, an analysis of the impact of this parameter on performance is required for the particular flow characteristics required in this work.

The drag coefficient criterion is not valid for this analysis, because it does not take into account the blade number increase for low values of pitch to axial chord ratios when the axial chord is kept constant. Consequently, the definition of total power dissipation across the stator is applied. The power dissipation is directly proportional to the ratio $C_d\,(b/t)$, thus, the variation of this parameter with the pitch to axial chord is shown in Figure 7 where the value $t/b = 0.851$ corresponds to the Zweifel criterion application.

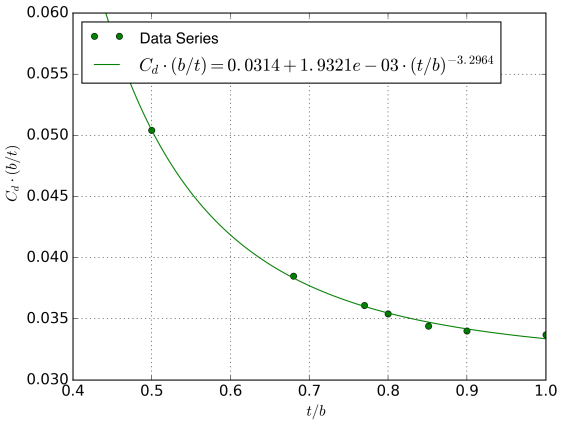

Figure 7: Total power dissipation equivalent parameter variation with pitch to axial chord ratio.

From the results obtained, the assessment of the optimum pitch to axial chord is not possible since the prediction that the total power dissipation equivalent ratio will keep decreasing for pitch to axial chord ratios higher than the presented range is acceptable. This means that, for the range studied, the contribution of friction losses was always greater than the contribution of separation losses.

Since a high pitch to axial chord ratio is undesirable when structural resistance is considered, i.e. a lower number of blades will imply higher forces applied on each blade, the Zweifel criterion result is adopted for the stator geometry.

With the mean radius geometry constraints defined, the final stator geometry may now be obtained. Due to manufacturing purposes, the axial chord is kept constant along the spanwise direction. There is a significant deviation verified between the outlet flow angle obtained in potential flow and the one obtained in viscous flow. This fact implies that the flow angle imposed during the potential flow design phase must be iterated until the outlet flow angle obtained in viscous flow is equal to the required angle. The final stator geometry is presented in Figure 8.

4. Rotor Design

The rotor design process differs from the one adopted for the stator as a consequence of the inlet conditions verified. Given the wide range of operat-

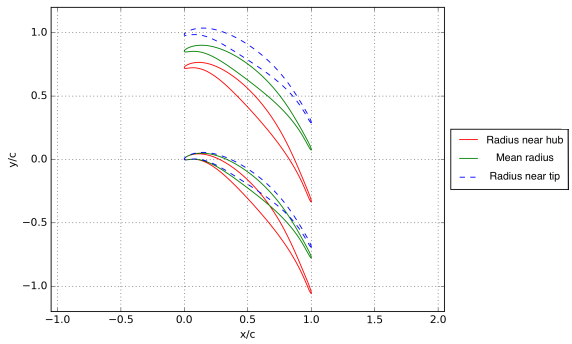

Figure 8: Final geometry for the three stator blade profiles designed.

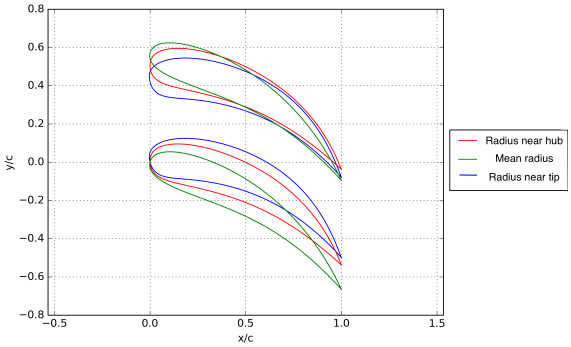

Figure 9: Final geometry for the three rotor blade profiles designed with the constant pressure coefficient criterion.

ing conditions required by a wave energy converter, factors like the variation of the inlet mass flow, the variation of the rotor rotational velocity and even perturbations on the flow upstream the stator might affect the efficiency of the flow deflection across the stator. Thus, the rotor inlet flow angle will have a deviation from the angle condition for which this component was designed.

Accordingly, the use of a known thickness distribution with a small radius at the leading edge is no longer adequate and a blade thickness distribution optimisation is required.

A pitch to axial chord ratio of 0.5 was selected as a requirement because for high ratio values the resultant geometries presented considerably large values of thickness near the leading edge, particularly for the first optimisation criterion.

The first criterion adopted for rotor blade design was a constant pressure coefficient in the highest percentage of chord possible. The advantage of this criterion relies on the fact that a zero pressure gradient allows a reliable control of the boundary layer growth and that separation losses effects are limited to a reduced region near the trailing edge where an intense adverse pressure gradient is verified. The final geometry results for this criterion are presented in Figure 9.

By analysing the obtained geometry, one might consider the high thickness obtained peculiar when compared to typical thickness distributions. To force a constant pressure coefficient means that the thickness at the leading edge will be also forced to increase in order to get the same pressure verified near the trailing edge, Figure 10. Without a viscous flow analysis, it is possible to conclude that the friction losses will be significant due to high velocities on the suction side of the blade profile.

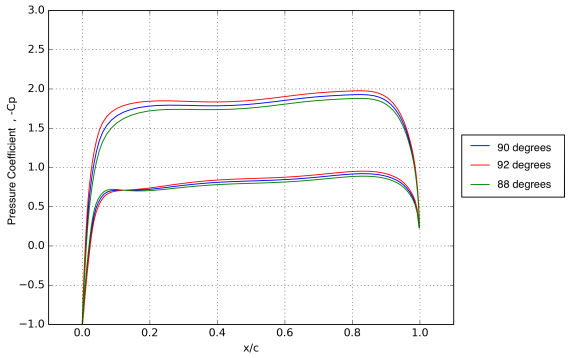

Figure 10: Pressure coefficient distribution in potential flow for the profile geometries obtained through the constant pressure coefficient criterion.

Note that the pressure coefficient has a slight slope due to the design iterations performed until the desired outlet angle was obtained in viscous flow done after the thickness optimization process.

The second criterion consist in imposing a favourable pressure gradient along the blade chord except near the trailing edge where a pressure recovery is necessary. The main objective with this new criteria is to keep separation losses low with the same previous assumption and, additionally, to reduce the velocity across the blade passage, i.e. to reduce friction losses. The final geometry results achieved after the optimization process and the outlet angle iteration process are presented in Figure 11.

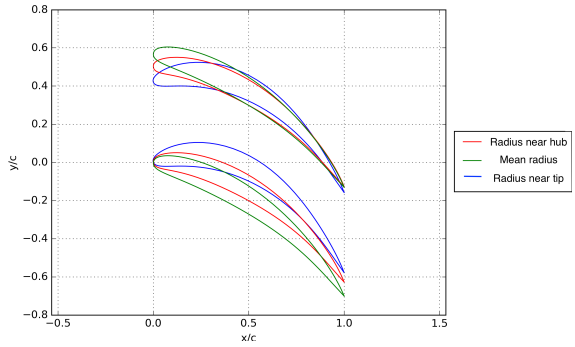

Figure 11: Final geometry for the three rotor blade profiles designed with the favourable pressure gradient criterion.

A significant reduction of the thickness near the leading edge is verified. The pressure coefficient distribution with this new criterion, Figure 12, predicts a reduction on friction losses since the pressure coefficient is now notably higher near the leading edge and even near the trailing edge a small difference is verified.

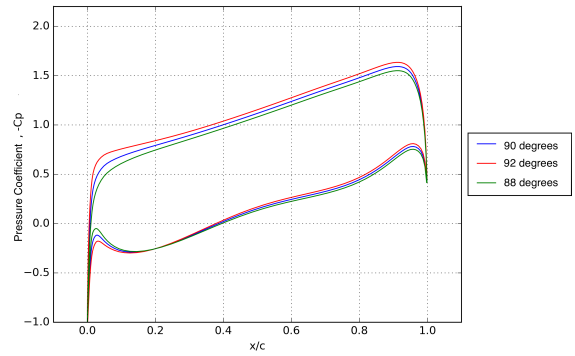

Figure 12: Pressure coefficient distribution in potential flow for the profile geometries obtained through the favourable pressure gradient criterion.

A quantitative analysis is required to verify if the performance improvement predicted is significant. Table 2 presents the drag coefficient values obtained with the viscous flow simulation.

Table 2: Drag coefficients at mean radius for each optimisation criterion adopted.

	Zero Gradient	Favourable Gradient
C_d	0.048	0.025

From the performance improvement with the favourable gradient criterion geometry, it is coherent to select this geometry to constitute a part on the final turbine design.

5. Numerical Study of the Three-dimensional Flow

The simulation of the three-dimensional flow is intended not only to verify the previous one-dimensional and two-dimensional design process but also to evaluate the interaction between the stator and the rotor. This will, then, allow an assessment of the global performance of the designed turbomachine.

The three-dimensional geometry is not completely defined at this point. The choice on the blade number for each component highly depends on the turbine geometry constraints and special attention is required to the aspect ratio of the blade. The stator and rotor interaction effects will determine the number of blades in each component as well as the relationship between these values and, also, the distance between the two components. The tip clearance is assumed to have a value of $0.5mm$ given the materials tolerance for manufacturing.

To introduce the three-dimensional flow analysis, a qualitative approach is advised. From the streamlines across blade passages presented in Figure 13, it is possible to observe the inlet axial flow being accelerated and deflected through the stator. Then, the flow enters in the rotor with an apparent axial relative velocity and exits the rotor with an approximately axial velocity. From the surface streamlines, it is possible to conclude that the secondary flow losses across the stator are negligible, although some losses might be verified across the rotor, more precisely near the hub. The surface streamlines also allow the visualisation of some tip leakage losses.

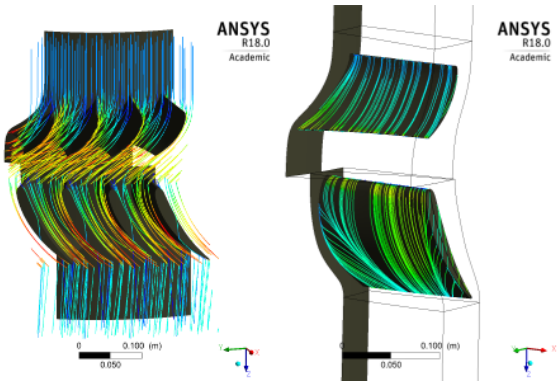

Figure 13: Streamlines across blade passages and surface stream lines.

The pressure variation and total pressure variation along the stream wise direction are shown in Figure 14 where location 1.1 corresponds to the stator leading edge and 2.0 to the rotor leading edge. The distribution verified the typical pressure distribution for a reaction turbine.

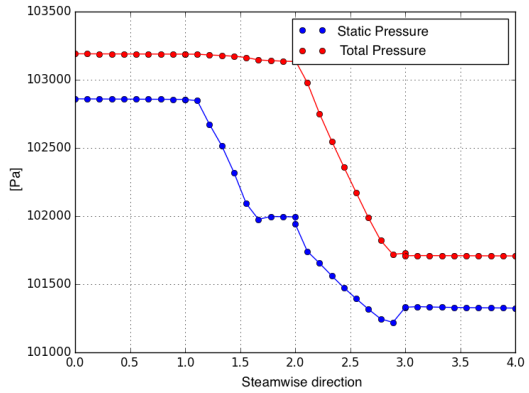

Figure 14: Pressure and total pressure variation along the streamwise direction.

The velocity contour at the mid-span position is presented in Figure 15. By analysing the stagnation point on the leading edge, it is clear that in both components a positive incidence is verified. Although the velocity deficit downstream caused by the presence of the blade is evident, there are no visible separation points on the blade surface for the two turbine components.

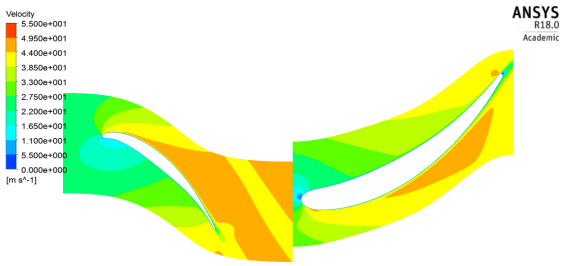

Figure 15: Velocity contours at the mid-span section.

Figure 16 shows the performance curve for the turbine stage, where a peak total-to-total efficiency of 90.7% is achieved. The total-to-total efficiency is defined by Equation 6 where h_0 is the total enthalpy, h_{0s} is the total isentropic enthalpy and the indexes 1 and 3 correspond to the inlet of the stator and to the outlet of the rotor, respectively.

$$\eta_{tt} = \frac{h_{01} - h_{03}}{h_{01} - h_{03_s}} \tag{6}$$

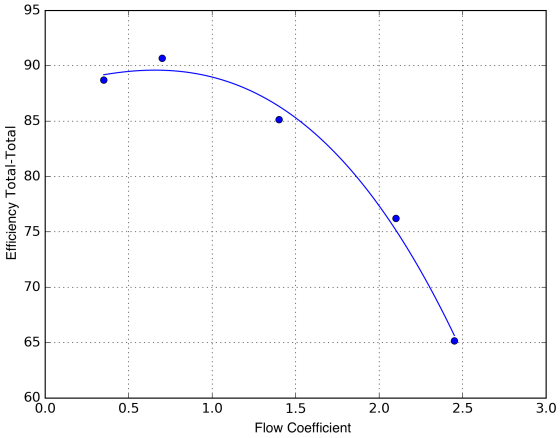

Figure 16: Performance curve.

6. Conclusions

The aim of this work is to design and to perform the numerical study of a stage turbine for a wave energy converter. Through the application of existent design methods, the criteria adopted to maximise the efficiency allowed the design of a final original geometry.

When compared to air turbines typically applied to oscillating water columns, the high efficiency of the turbine designed is quite notable. Although in real conditions the turbine might not be operating in peak efficiency conditions, the wide and flat performance curve computed still guarantees good performance characteristics.

Future work proposals include a cost-benefit analysis for a twin-rotor turbine design and a validation of the numerical results through experimental essays.

References

[1] S. Barstow, G. Mørk, and D. Mollison. The Wave Energy Resource. In *Ocean Wave Energy: Current Status and Future Perspectives*, chapter 4, pages 93–132. Springer, Berlim, 2004.

[2] A. F. O. Falcão and J. C. C. Henriques. Oscillating-water-column wave energy converters and air turbines: A review. *Renewable Energy*, 85:1391–1424, 2016.

[3] R. P. F. Gomes, J. C. C. Henriques, L. M. C. Gato, and A. F. O. Falcão. Multi-point aerodynamic optimization of the rotor blade sections of an axial-flow impulse air turbine for wave energy conversion. *Energy*, 45(1):570–580, 2012.

[4] K. Mala, J. Jayaraj, V. Jayashankar, T. M. Muruganandam, S. Santhakumar, M. Ravindran, M. Takao, T. Setoguchi, K. Toyota, and S. Nagata. A twin unidirectional impulse turbine topology for OWC based wave energy

plants - Experimental validation and scaling. *Renewable Energy*, 36(1):307–314, 2011.

[5] S. L. Dixon and C. A. Hall. *Fluid Mechanics and Thermodynamics of Turbomachinery*. Butterworth-Heinemann/Elsevier, 2014.

[6] H. R. M. Craig and H. J. A. Cox. Performance estimation of axial flow turbines. *Proceedings of the Institution of Mechanical Engineers*, 185:407–424, 1970.

[7] J. C. C. Henriques, F. Marques, A. I. Estanqueiro, and L. M. C. Gato. Design of a new urban wind turbine airfoil using a pressure-load inverse method. *Renewable Energy*, 34(12):2728–2734, 2009.

[8] B. Lakshminarayana. *Fluid Dynamics and Heat Transfer of Turbomachinery*. John Wiley & Sons, Inc., 1996.

[9] F. R. Menter. Two-Equation Eddy-Viscosity Turbulence Models for Engineering Applications. *American Institute of Aeronautics and Astronautics Journal*, 32(8):1598–1605, 1994.

[10] J. H. Horlock. *Axial Flow Turbines: Fluid Mechanics and Thermodynamics*. Krieger Pub Company, 1966.